Implementation of Oxy-Fuel Combustion (OFC) technology in a Gasoline Direct Injection (GDI) engine fuelled with gasoline-ethanol blends

Xiang Li [a,*], Yiqiang Pei [b], Dayou Li [a], Tahmina Ajmal [a], Abdel Aitouche [c, d], Raouf Mobasheri [c, d], Zhijun Peng [e,*]

[a] School of Computer Science and Technology, University of Bedfordshire, LU1 3JU, UK

[b] State Key Laboratory of Engines, Tianjin University, Tianjin 300072, China

[c] Univ. Lille, CNRS, Centrale Lille, UMR 9189 - CRIStAL - Centre de Recherche en Informatique Signal et Automatique de Lille, F-59000 Lille, France

[d] Junia, Smart Systems and Energies, F-59000 Lille, France

[e] School of Engineering, University of Lincoln, Lincoln, UK

ABSTRACT

Nowadays, to mitigate the global warming problem, the requirement of carbon neutrality has become more urgent. Oxy-Fuel Combustion (OFC) has been proposed as a promising way of Carbon Capture and Storage (CCS) to eliminate Carbon Dioxide (CO_2) emissions. This article explores the implementation of OFC technology in a practical Gasoline Direct Injection (GDI) engine fuelled with gasoline-ethanol blends, including E0 (gasoline), E25 (25% ethanol, 75% is gasoline in mass fraction) and E50 (50% ethanol, 50% is gasoline in mass fraction). The results show that with a fixed spark timing, φ_{CA50} (where 50% fuel is burned) of E50 and E25 is about 4.5 degrees and 1.9 degrees later than that of E0, respectively. Ignition delay (θ_F) and combustion duration (θ_C) can be extended with the increase of ethanol fraction in the blended fuel. With the increase of Oxygen Mass Fraction (OMF) from 23.3% to 29%, equivalent Brake Specific Fuel Consumption ($BSFC_E$) has a benefit of 2.12%,

1.65% and 1.51% for E0, E25 and E50, respectively. The corresponding increase in Brake Specific Oxygen Consumption (BSOC) is each 21.83%, 22.42% and 22.58%. Meantime, θ_F, θ_C and Heat Release Rate (HRR) are not strongly affected by OMF. With the increase of OMF, the increment of θ_F is each 0.7 degrees, 1.8 degrees and 2.2 degrees for E0, E25 and E50. θ_C is only extended by 1 degree, 1.1 degrees and 1.4 degrees, respectively. Besides, by increasing intake temperature (T_I) from 298 K to 358 K under all the fuel conditions, $BSFC_E$ and BSOC present slight growth trends; θ_F and θ_C are slightly reduced; meantime φ_{CA50}, φ_{Pmax} (crank angle of peak cylinder pressure) and the position of HRR peak are advanced by nearly 1 degree.

KEYWORDS

Oxy-Fuel Combustion (OFC); Gasoline Direct Injection (GDI) engine; Gasoline-ethanol blends; Simulation.

1. INTRODUCTION

Climate change, particularly global warming, has been a serious problem, which causes a wide range of effects on the world. Hence, carbon neutrality has been proposed as an urgent need to limit global warming by reducing Greenhouse Gas (GHG) emissions.[1]- [4] Aiming at reducing the emissions of primary long-lived GHG Carbon Dioxide (CO_2), Oxy-Fuel Combustion (OFC) technology is helpful to achieve Carbon Capture and Storage (CCS) in conventional Internal Combustion Engine (ICE) fuelled with fossil fuels.[5]-[8] OFC technology was proposed by Yaverbaum,[5] which chemical reaction process is shown in Equation (1). It presents that the major advantage of OFC is to avoid emissions related with nitrogen element. Hence, engine exhaust emissions are almost CO_2 and H_2O. Then, H_2O can be condensed and separated by a condenser and

a gas/water separator. A portion of remained CO_2 can be recirculated back to cylinders for utilisation. Meantime, the rest of CO_2 could be compressed, captured and stored. The physicochemical properties of CO_2 and nitrogen are listed in Table 1, which make OFC quite different from Conventional Air Combustion (CAC).[9][10]

$$C_xH_y + \left(x + \frac{y}{4}\right) O_2 \rightarrow xCO_2 + \frac{y}{2} H_2O \quad (1)$$

Table 1. Gas physicochemical properties at 1000 K and 0.1 MPa [9][10]

Property	CO_2	nitrogen	Ratio (CO_2/nitrogen)
Molecular weight	44	28	1.57
Density (kg/m^3)	0.5362	0.3413	1.57
Kinematic viscosity (m^2/s)	7.69e-5	1.2e-4	0.631
Specific heat capacity (kJ/kg K)	1.2343	1.1674	1.06
Thermal conductivity (W/m K)	7.057e-2	6.599e-2	1.07
Thermal diffusivity (m^2/s)	1.1e-4	1.7e-4	0.644
Mass diffusivity of O_2 (m^2/s)	9.8e-5	1.3e-4	0.778
Prandtl number	0.7455	0.7022	1.06
Emissivity and absorptivity	> 0	~ 0	-

In 1999, Bilger [6] introduced a novel system named Internal Combustion Rankine Cycle (ICRC), initiating the application of OFC technology into Spark Ignition (SI) ICE. In the ICRC system, CO_2 with oxygen enters into engine combustion chambers. The other prominent characteristic is that water is directly injected into chambers near the top dead centre to control combustion. Over the last decade, Wu et al.[11]-[14] provided valuable inputs into OFC research, which indicated that the power, fuel economy and emissions could be improved through optimisation strategies in the ICRC Port Fuel Injection (PFI) engine fuelled with propane. Li et al.[15],[16] explored the potential of intake charge to optimise combustion and performance of OFC SI engine fuelled with gasoline.

In summary, most studies about OFC technology in SI engines mainly focused on PFI engines fuelled propane. A minority of studies have been conducted in Gasoline Direct Injection (GDI) engines. GDI technique is widely known to be the mainstream of SI engines.[17]-[22] Furthermore, in order to meet the more stringent standards by reducing vehicular emissions, alcohols have been promising alternative fuels and are widely used as fuel blending components nowadays. [23]-[29] However, it is still unknown about the impacts of OFC implementation in a GDI engine fuelled with gasoline-ethanol blends.

Hence, the study purpose is to explore and provide a deeper understanding of the implementation of OFC technology in a practical GDI engine fuelled with gasoline-ethanol blends. This study is a small part of an ongoing 'RIVER' project funded by European Regional Development Fund (ERDF), which aims to develop a novel non-carbon riverboat powered by ICE with conventional hydrocarbon liquid fuels. In this project, a designed system of OFC with CCS in the application of ICE can be depicted in Figure 1. In order to achieve non-carbon emissions, pure oxygen is mixed with recirculated exhaust gas (CO_2) prior to entering engine combustion chambers. Meantime, the excess CO_2 would be captured and eventually stored in a storage tank.

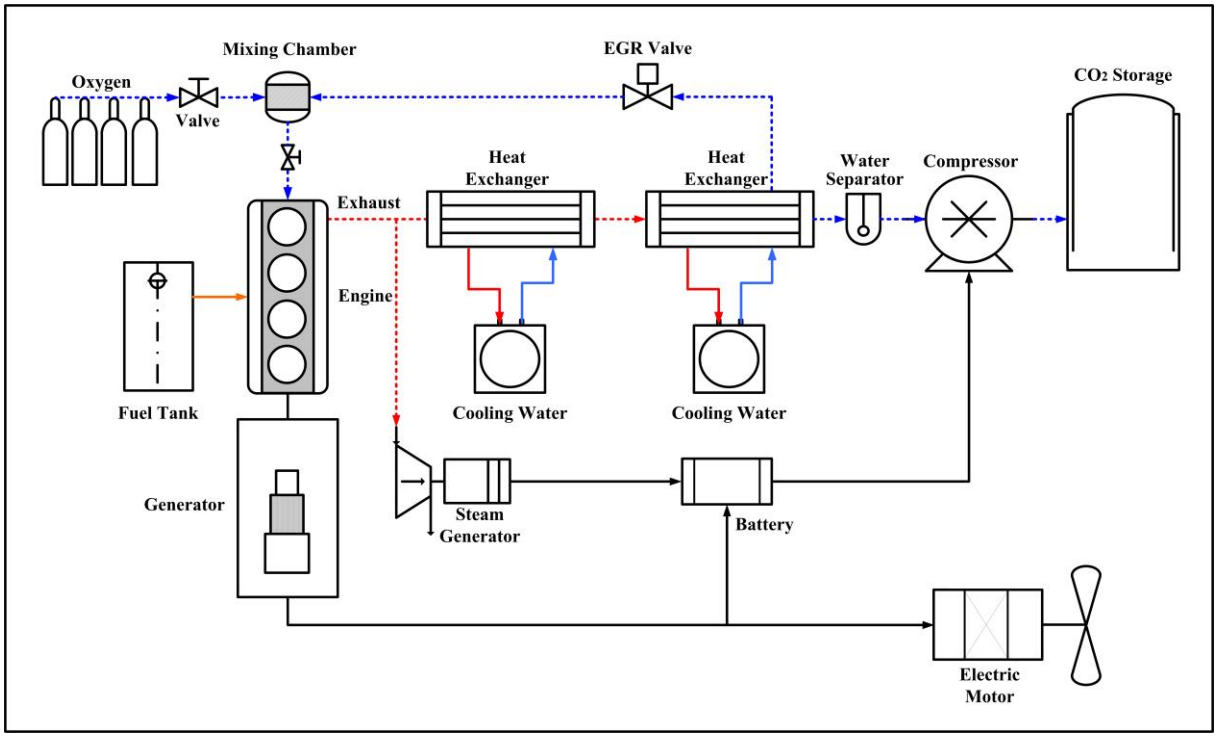

Figure 1. Schematic of OFC in the application of ICE with CCS

2. SIMULATION METHODOLOGY

2.1 Engine Testbed

The numerical study is performed with a turbocharged 2.0-litre GDI engine, which specifications and testbed are illustrated in Table 2 and Figure 2, respectively.

The required data for model validation was obtained from the engine testbed under CAC mode. The engine's speed and torque can be accurately controlled and measured by a programmable Electronic Control Unit (ECU) and an electrical dynamometer. In addition, spark-plug type pressure sensors (AVL-GH13Z), a charge amplifier (Kistler 5018A) and a combustion analyser (AVL 641) were utilised to measure, analyse and record the transient cylinder pressure signals. The cylinder pressure should be averaged by 200 consecutive cycles to reduce the deviation of cycle-to-cycle variations. According to Holman's root mean square method, the uncertainties of some items are listed in Table 3.[30] Besides, the spark timings were optimised to be the minimum advance for Maximum Brake Torque (MBT) or the Knock Limited Spark Advance (KLSA). The used fuels in this study

include E0 (gasoline), E25 (25% ethanol, 75% is gasoline in mass fraction) and E50 (50% ethanol, 50% is gasoline in mass fraction), which are mixed and ensure to completely miscible before the test. The fuel properties of used gasoline and ethanol are presented in Table 4.

Table 2. Engine specifications

Items	Content
Engine type	4-cylinder, 4-stroke
Bore × Stroke (mm)	82.5 × 92
Displacement (L)	2.0
Injection type	GDI
Intake type	Turbocharged
Compression ratio	9.6:1
Rated speed (rpm)	5500
Rated power (kW)	160
Maximum Torque (N·m)	320

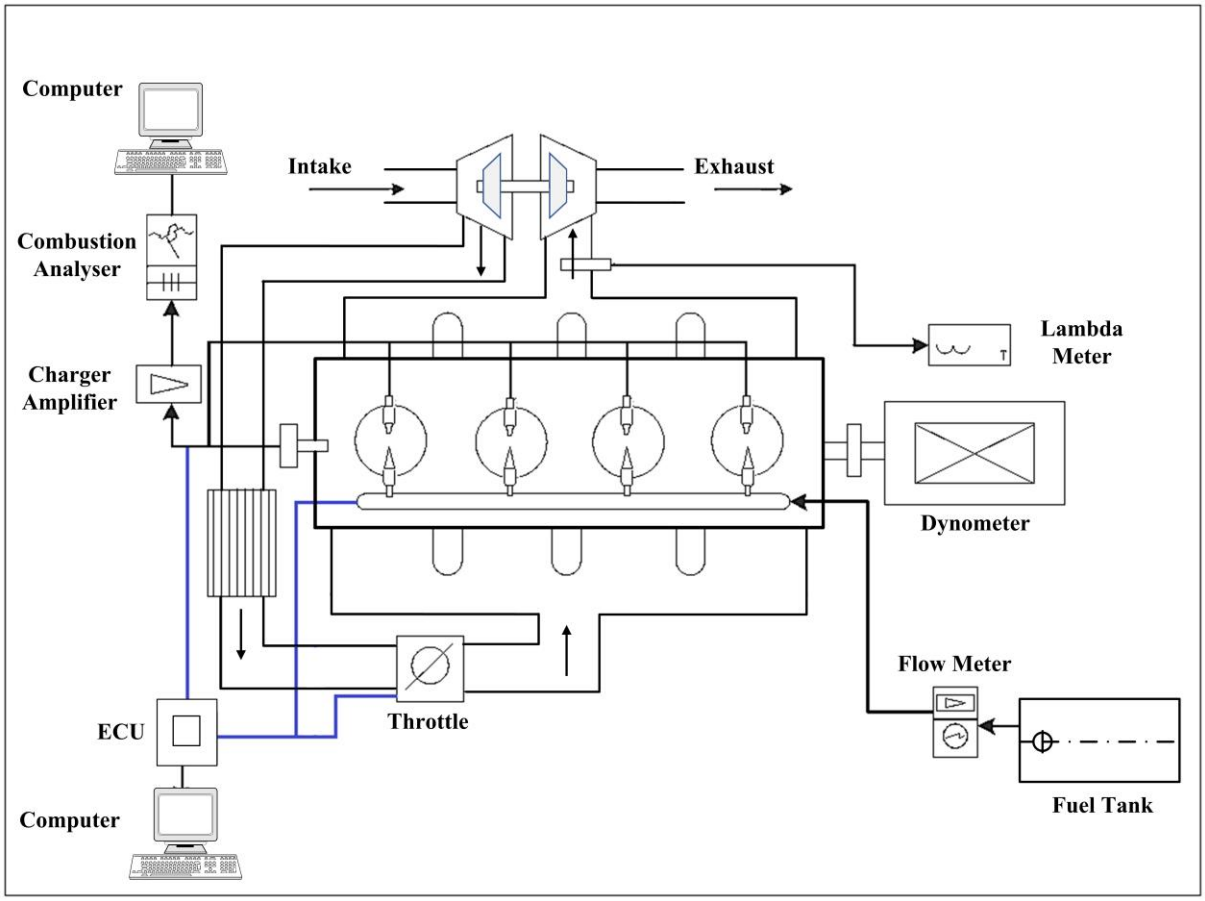

Figure 2. Schematic of the engine testbed

Table 3. Uncertainties of measured parameters

Measured Parameters	Uncertainty (%)
Engine speed	± 0.1
BMEP	± 0.1
BSFC	± 0.2
Cylinder Pressure	± 0.1
Lambda	± 0.3
Coolant temperature	± 0.4
Intercooler output temperature	± 0.4

Table 4. Fuel properties

Fuel type	Ethanol	Gasoline
Chemical formula	C_2H_5OH	C5-C12
Relative molecular mass	46	95-120
Gravimetric oxygen content (%)	34.78	< 1
Research octane number	107	95
Density (20 ℃) (kg/L)	0.789	0.73
Dynamic viscosity (20 ℃) (mPa·s)	1.2	0.52
Kinematic viscosity (20 ℃) (mm^2/s)	1.52	0.71
Surface tension (20 ℃) (N/m)	21.97	22
Boiling range (℃)	78	30-200
Low heating value (kJ/kg)	26900	44300
Latent heat of vaporisation (kJ/kg)	840	370
Laminar flame speed (20 ℃) (m/s)	0.5	0.33
Stoichiometric air-fuel ratio	8.95	14.7

2.2 Model Description and Research Approach

The one-dimensional model of this numerical study is established by GT-Power, which is very common for academics in the research of SI engines.[31]-[33] The main submodels are 'Woschni model' [34] and 'SI turbulent flame combustion model'.[35] The heat transfer coefficient h and laminar flame speed S_L can be presented in Equation (2) and Equation (3), respectively.

$$h = 110d^{-0.2}P^{0.8}T^{-0.53}[C_1c_m + C_2\frac{V_ST_1}{P_1V_1}(P - P_0)]^{0.8} \quad (2)$$

Here, h denotes heat transfer coefficient; d denotes diameter of the cylinder bore; P denotes

cylinder pressure; T denotes in-cylinder mean gas temperature; C_1 denotes a constant related to airflow velocity coefficient; C_2 denotes a constant related to combustion chamber; c_m denotes mean piston speed; V_S denotes cylinder volume; P_0 denotes the cylinder pressure when the engine is started. T_1, P_1 and V_1 are cylinder temperature, pressure and volume at the beginning of compression, respectively.

$$S_L = [B_m - B_\delta(\delta - \delta_m)^2]\left(\frac{T_u}{T_{ref}}\right)^\alpha \left(\frac{p}{p_{ref}}\right)^\beta f(D) \quad (3)$$

Here, S_L denotes laminar flame speed; B_m denotes maximum laminar speed; B_δ denotes laminar speed roll-off value; δ denotes in-cylinder equivalence ratio; δ_m denotes equivalence ratio at maximum speed; T_u denotes unburned gas temperature; T_{ref} denotes 298 K; p denotes pressure; p_{ref} denotes 101.325 kPa; α denotes temperature exponent; β denotes pressure exponent; $f(D)$ denotes dilution effect.

In this research, fuelled with E0, E25 and E50, the engine runs at 1500 revolutions per minute (rpm) with 10 bar Brake Mean Effective Pressure (BMEP), representing a mid-high load of engine operating condition. The research approach of this study is illustrated in Figure 3.

First, model validation is completed based on the experimental data. Second, the optimisation of OFC performance by changing spark timing is conducted. In the meantime, the throttle opening angle and stoichiometric air-fuel ratio are held constant. Third, the performance optimisation by changing Oxygen Mass Fraction (OMF) is analysed. When OMF changes, the throttle opening angle remains unchanged and the spark timings should be optimised to be MBT under each OMF condition. Last, simulation work is conducted to try to optimise engine performance by changing intake temperature.

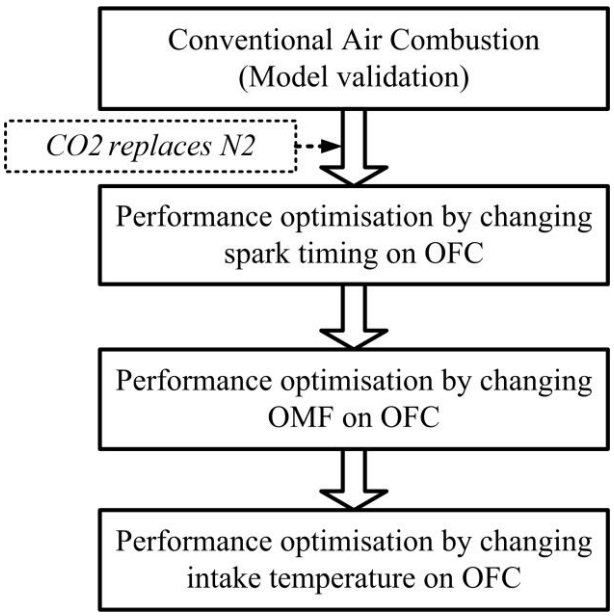

Figure 3. Flow chart of the research approach

In this study, ignition delay (θ_F) denotes the Crank Angle (CA) interval between spark timing and φ_{CA10} (where 10% fuel is burned). Combustion duration (θ_C) denotes the CA interval between φ_{CA10} and φ_{CA90} (where 90% fuel is burned). Besides, φ_{CA50}, T_M and φ_{Pmax} are introduced to denote the CA where 50% fuel is burned, the maximum in-cylinder temperature and the CA of peak cylinder pressure. Brake Specific Oxygen Consumption (BSOC), equivalent Brake Specific Fuel Consumption ($BSFC_E$) and $lambda_{O2}$ are introduced in Equations (4), (5) and (6), respectively.

$$\mathrm{BSOC} = \frac{\tau_O \times 1000}{P} \tag{4}$$

$$\mathrm{BSFC_E} = \frac{\tau_F \times 1000}{P} \times \frac{(\omega_E \times H_E) \times (\omega_G \times H_G)}{H_G} \tag{5}$$

$$lambda_{O2} = \frac{\tau_O}{\tau_{ost}} \tag{6}$$

Here, P (kW) denotes the engine brake power. τ_O (kg/h) and τ_F (kg/h) is the consumption rate of oxygen and fuel under actual conditions, respectively. τ_{ost} (kg/h) denotes the oxygen mass flow rate at the stoichiometric condition. ω_E and ω_G are the mass fraction of ethanol and gasoline in the fuel, respectively. H_E and H_G are the low heating value of ethanol and gasoline, respectively.

3. RESULTS AND DISCUSSION

3.1 Model Validation

Figure 4 presents the model validation by a comparison of cylinder pressure between experiment and simulation results under E0, E25 and E50 conditions. It can be seen that the curves are in good agreement under all the conditions. The locations and magnitudes of the curves' peaks have been well predicted. It can indicate that this model is capable of being used for this numerical research.

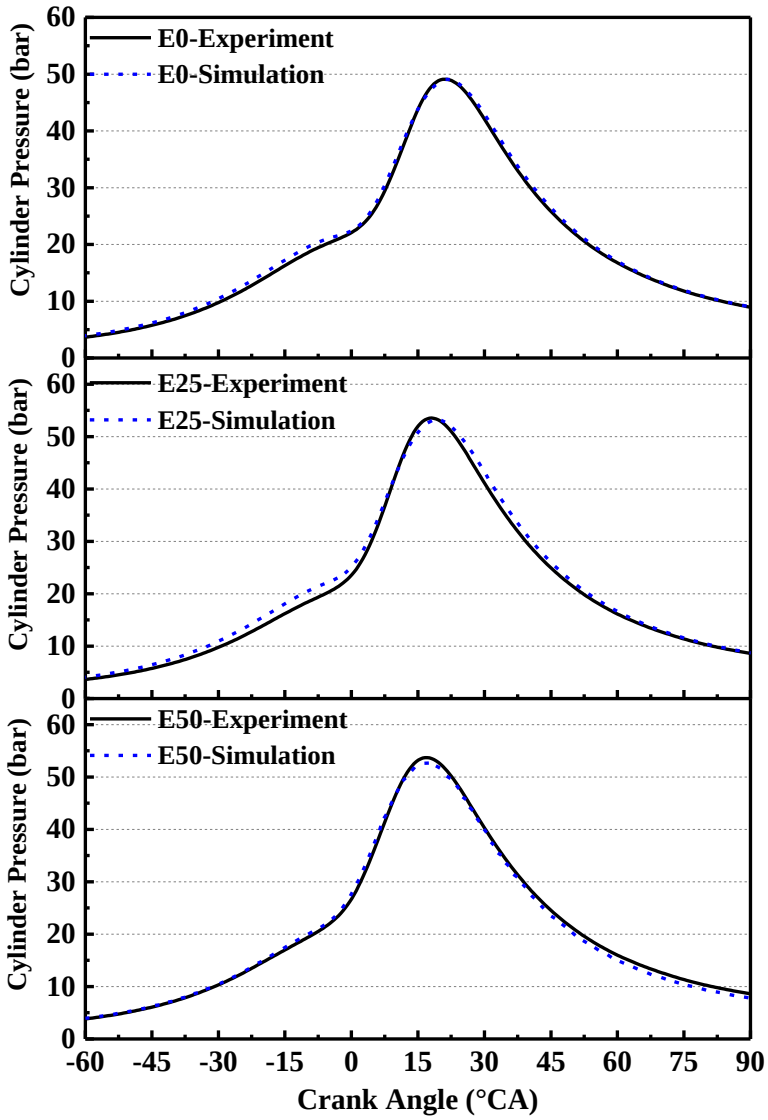

Figure 4. Comparison of cylinder pressure between experimental and simulation results

3.2 Performance Optimisation by Changing Spark Timing

This section shows the effects of spark timing on engine combustion performance. Meantime, OMF and T_I are kept at 23.3% and 298 K, respectively.

Figure 5 presents the effects of spark timing on $BSFC_E$ and φ_{CA50}. It can be observed that with the advance of spark timing from -40 ºCA to -68 ºCA, the overall trend of $BSFC_E$ initially has a small reduction and then increases. For E0, E25 and E50, the lowest $BSFC_E$ is each 317.62 g/kWh, 306.48 g/kWh and 295.82 g/kWh, which is achieved with the spark timing of -52 ºCA, -54 ºCA and -58 ºCA.

These differences can be observed with the combustion phasing characterised by φ_{CA50}, θ_F and θ_C. The corresponding φ_{CA50} with MBT timing is 4 ºCA, 4.5 ºCA and 4.4 ºCA, respectively. Besides, there is a clear contrast between the overall trend of θ_F and θ_C as shown in Figure 6. By advancing spark timing from -40 ºCA to -68 ºCA, θ_F increases by about 11.2 degrees, 11.2 degrees and 11.1 degrees for E0, E25 and E50, respectively. In the meantime, θ_C has a corresponding decline by 9.2 degrees, 11.2 degrees and 14.5 degrees. It can be explained by Heat Release Rate (HRR), an example case with E25 of Figure 7 also demonstrates that the combustion phasing is very sensitive to spark timing which leads to a considerable variation in both the location and magnitude of HRR.

Another important result presented in this section is that with a fixed spark timing, the φ_{CA50} of E50 and E25 is about 4.5 degrees and 1.9 degrees later than that of E0, as shown in Figure 5. Meantime, θ_F and θ_C can be extended with the increase of ethanol fraction in the blended fuel. The changes can be attributed to two main reasons by fuel properties, as shown in Table 4. First, the latent heat of vaporisation of ethanol is significantly higher than that of gasoline, leading to a stronger cooling effect and suppression of combustion rate. The T_M of E50 is the lowest among the three fuel, while that of E0 is the highest, as shown in Figure 8. Second, the laminar flame speed of ethanol is higher than that of gasoline, which would promote combustion rate and complete combustion.

However, the benefit cannot counteract the negative effects of high latent heat of vaporisation of ethanol in this operating condition.

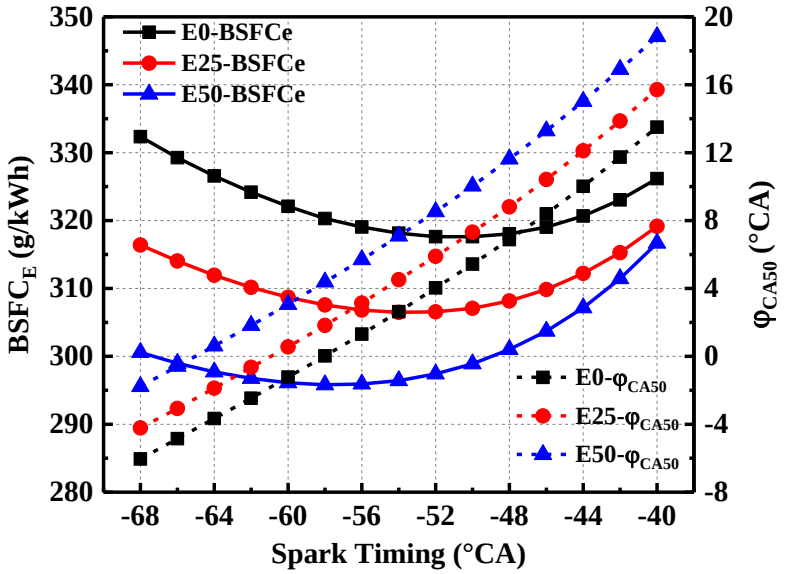

Figure 5. Effects of spark timing on $BSFC_E$ and φ_{CA50}

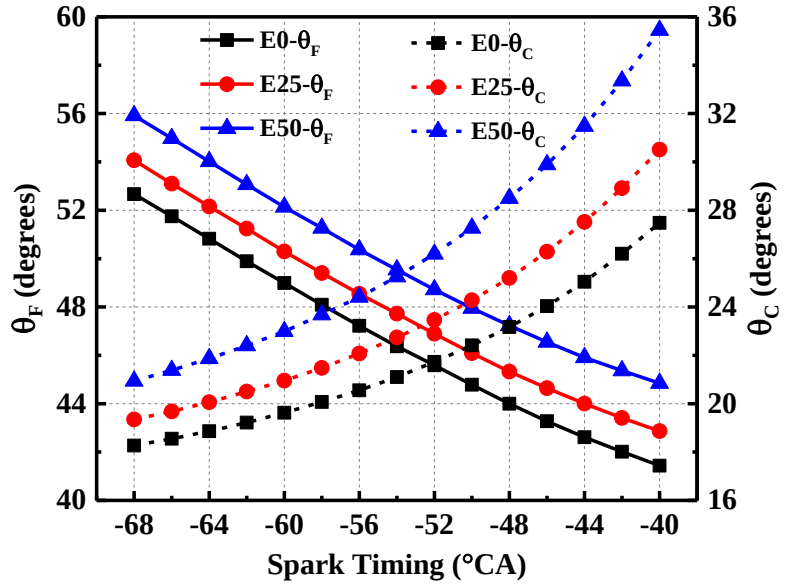

Figure 6. Effects of spark timing on θ_F and θ_C

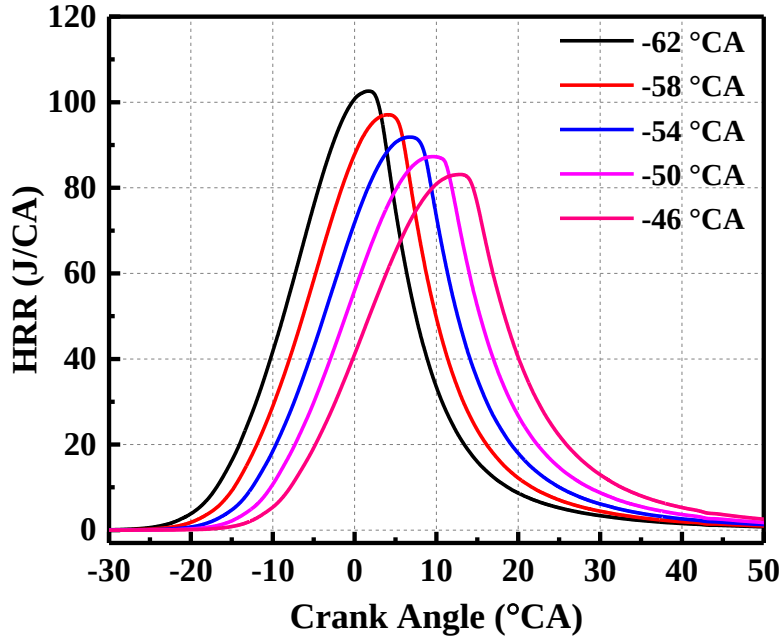

Figure 7. Effects of spark timing on HRR (E25)

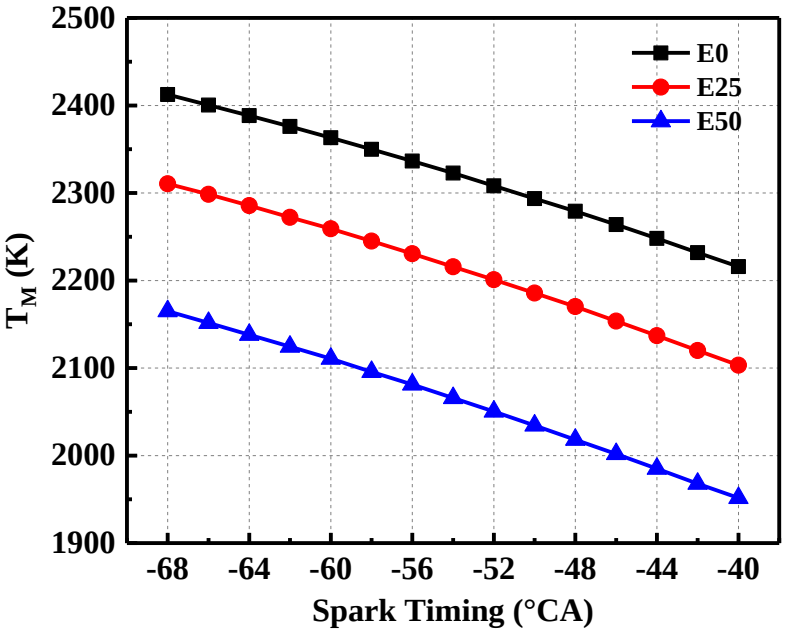

Figure 8. Effects of spark timing on T_M

3.3 Performance Optimisation by Changing OMF

This section presents the optimisation results on engine combustion performance by changing OMF. Furthermore, T_I is kept at 298 K, and MBT timing is applied for all operating conditions.

Figure 9 shows the effects of OMF on $BSFC_E$ and BSOC. The OMF is limited to 29% in this study because the cost of oxygen supplements should be considered in practical applications. It is set

to be 23.3%, 25%, 27% and 29%, and the corresponding $lambda_{O2}$ is each 1, 1.073, 1.159 and 1.245. Furthermore, the spark timings are optimised to be MBT under each OMF condition.

It can be observed that both the $BSFC_E$ and BSOC are sensitive to the change of OMF. With the increase of OMF to 29%, the reduction of $BSFC_E$ is each 6.74 g/kWh, 5.06 g/kWh and 4.47 g/kWh for E0, E25 and E50, which is a saving rate of 2.12%, 1.65% and 1.51%. This benefit is mainly because the specific heat ratio is heightened with the increased OMF, resulting in higher conversion efficiency and stronger work per unit mass of fuel.[35] Besides, the general trend of BSOC is opposite to that of $BSFC_E$. Under the condition of E0, E25 and E50, there is an increase of 21.83%, 22.42% and 22.58% in BSOC, respectively. It means that the growing consumption of oxygen should also be considered under higher OMF conditions. Hence, the cost from higher BSOC should be considered with the increase of OMF.

Figure 10 presents the effects of OMF on θ_F and θ_C. It can be seen that both θ_F and θ_C are not strongly affected by OMF. With the increase of OMF, the increment of θ_F is each 0.7 degrees, 1.8 degrees and 2.2 degrees for E0, E25 and E50. Meantime, θ_C is only extended by 1 degree, 1.1 degrees and 1.4 degrees, respectively. This is mainly because by increasing OMF to 27% or 29%, the lean fuel-air mixture ($lambda_{O2} > 1.1$) would have a negative impact on laminar burning velocity, although the impact is partially offset by the influence of decreasing CO_2 fraction in the intake.[35],[36] This can also be further explained by HRR, an example case with E25 in Figure 12. It demonstrates that there is no apparent discrepancy in HRR by increasing OMF. The peak of HRR is just slightly decreased by 2.5 J/CA and postponed by 1.5 degrees.

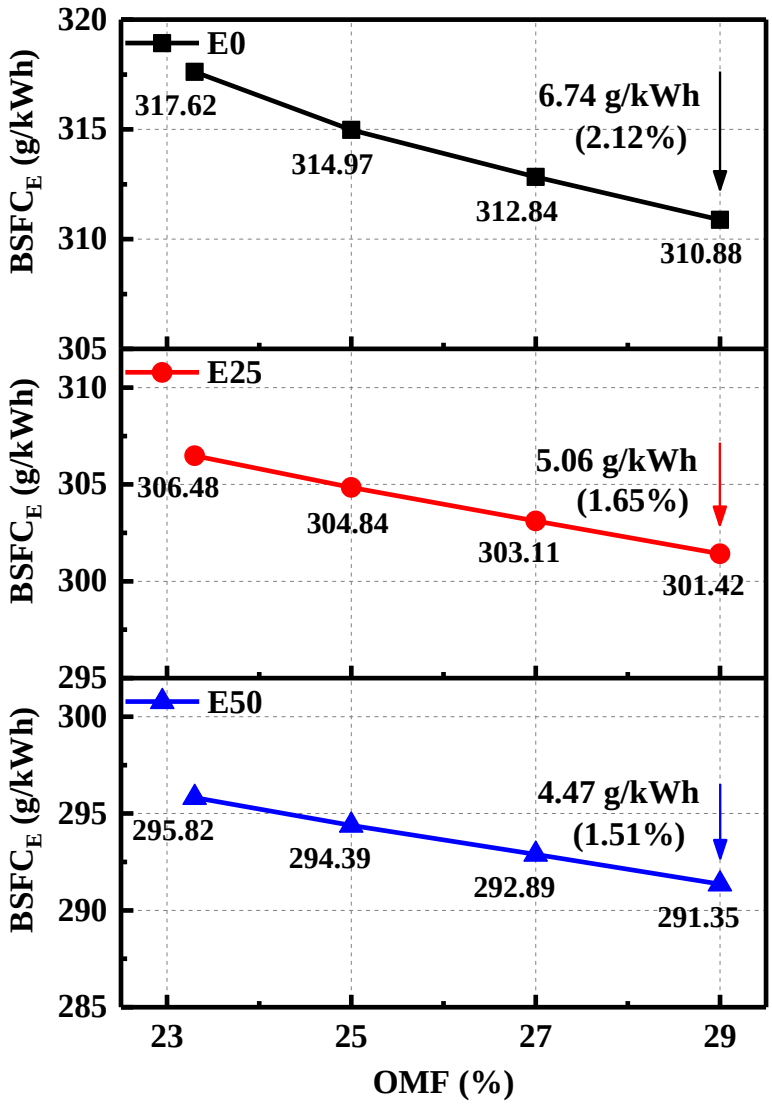

Figure 9. Effects of OMF on BSFC$_E$

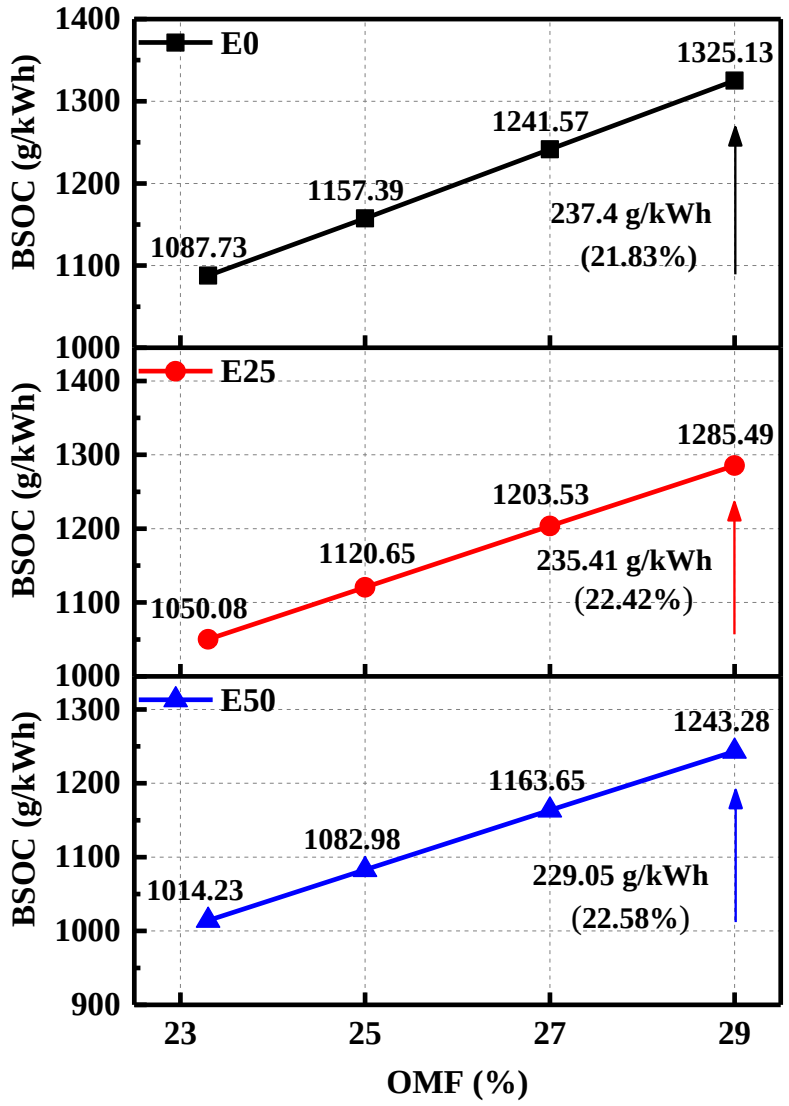

Figure 10. Effects of OMF on BSOC

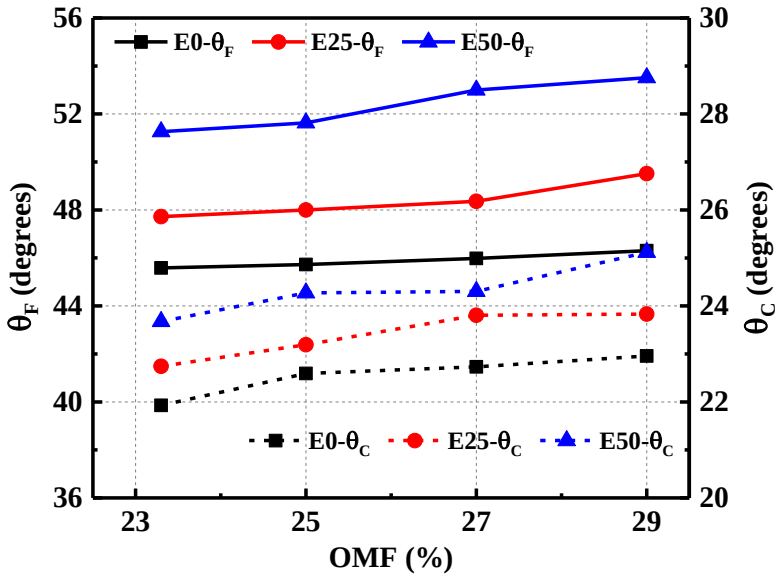

Figure 11. Effects of OMF on θ_F and θ_C

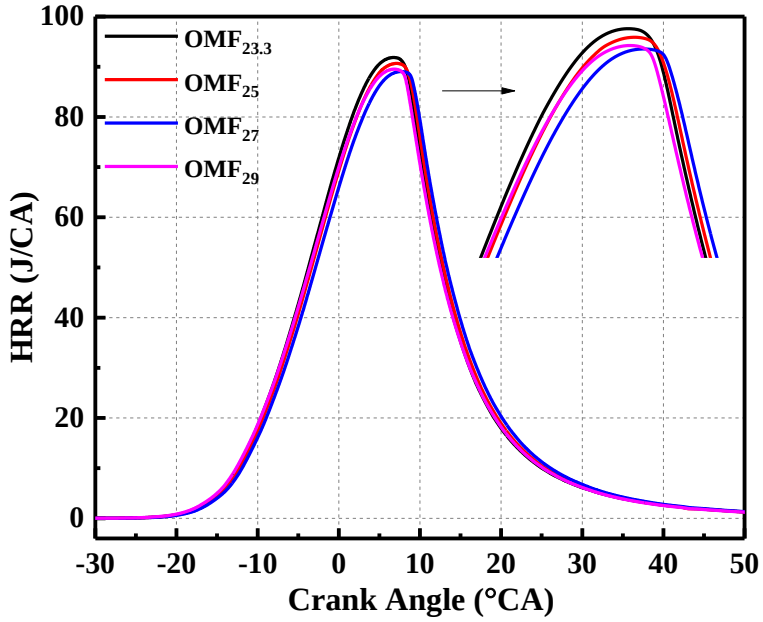

Figure 12. Effects of OMF on HRR (E25)

3.4 Performance Optimisation by Changing Intake Temperature

In this section, the simulation work is conducted to try to optimise engine performance by changing intake temperature from 298 K to 358 K. Furthermore, the OMF conditions are selected with 23.3% and 29%, the spark timings are optimised to be MBT.

Figure 13 and Figure14 shows the effects of T_I on BSFC$_E$ and BSOC, respectively. It can be seen that with the increase of T_I from 298 K to 358 K, all the curves of BSFC$_E$ and BSOC present steady but slight growth trends. Hence, an analysis of normalisation is also depicted in Figure13 to show the comparisons with the condition of T_I = 298 K. The average increase rate is respectively 0.28% and 0.23% for OMF = 23% and OMF = 29%. This is mainly because that intake density will be reduced by increasing T_I under a fixed opening angle of engine throttle.

In the meantime, the combustion phasing will be slightly affected by changing T_I under E0, E25 and E50 fuel conditions. As shown in Figure15 and Figure 16, by increasing T_I from 298 K to 358 K, θ_F and θ_C will be reduced by around 0.7 degrees. φ_{CA50}, φ_{Pmax} and the position of HRR peak

will be advanced by nearly 1 degree. This is principally because the atomisation of fuel droplets could be enhanced with a higher temperature intake.

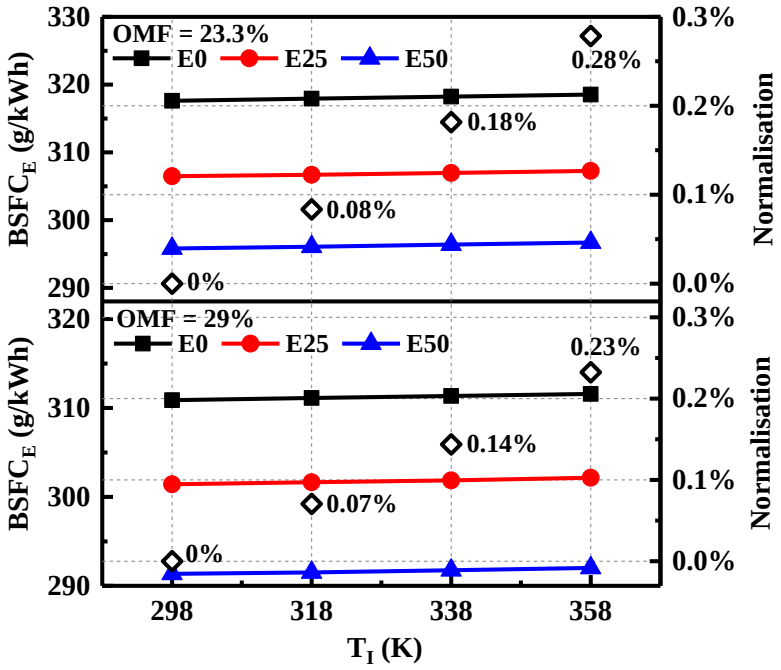

Figure 13. Effects of T_I on BSFC$_E$

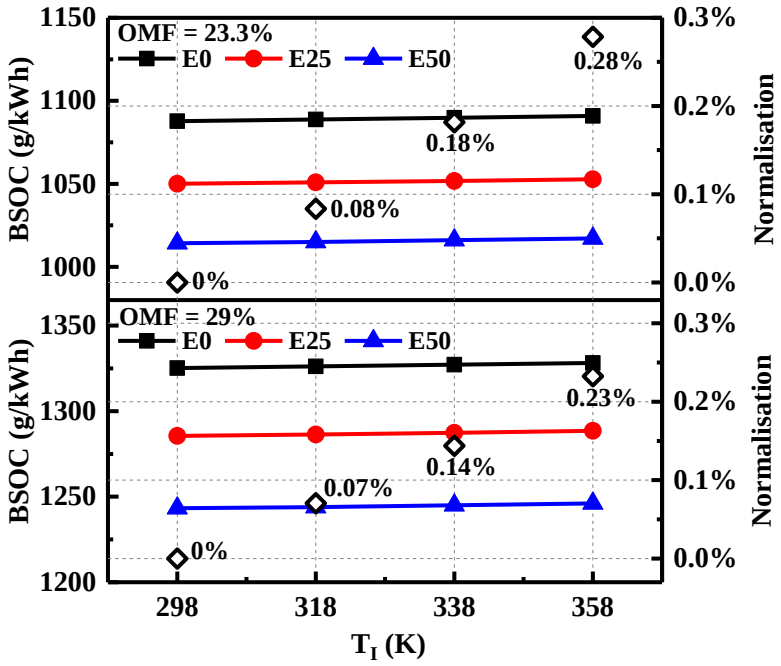

Figure 14. Effects of T_I on BSOC

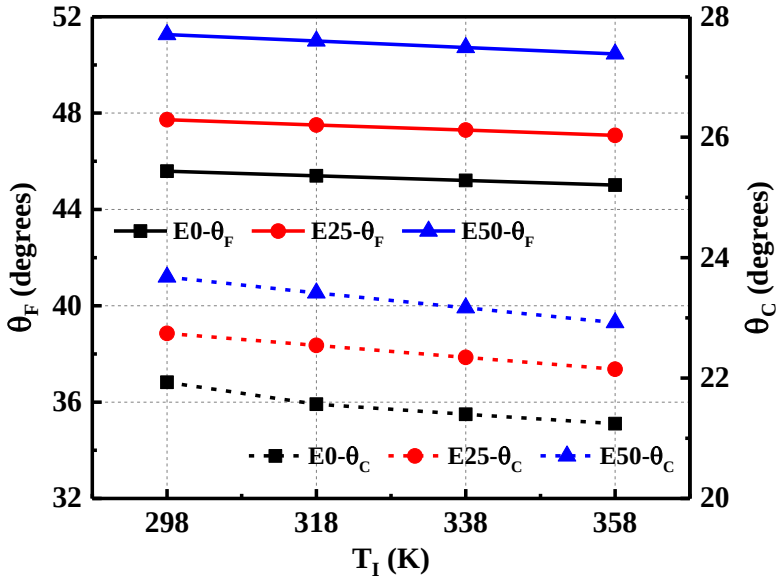

(a) OMF = 23.3%

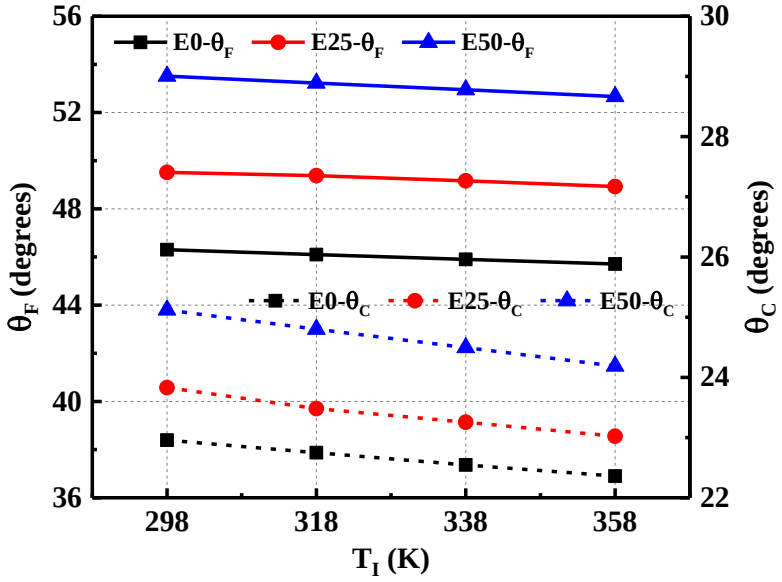

(b) OMF = 29%

Figure 15. Effects of T_I on θ_F and θ_C

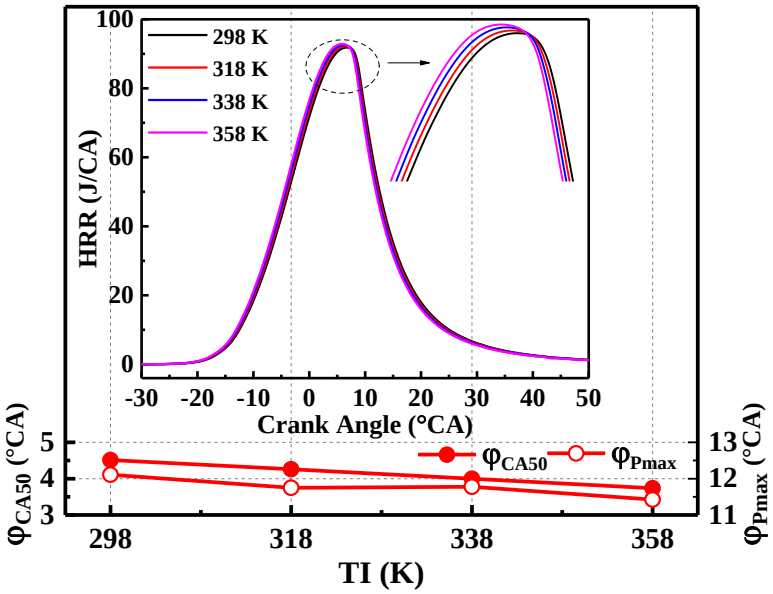

Figure 16. Effects of T_I on HRR, φ_{CA50} and φ_{Pmax} (E25; OMF = 23.3%)

4. CONCLUSIONS

This work belongs to the 'RIVER' project to develop a non-carbon riverboat powered by ICE with conventional hydrocarbon liquid fuels, which is expected to make a valuable contribution to carbon neutrality in the world. The findings of this work not only provide a critical analysis on the implementation of OFC technology in a practical GDI engine fuelled with gasoline-ethanol blends, but also continue to contribute to this growing area by exploring the methods of improving the efficiency of OFC SI engines. The major conclusions in this article can be summarised as follows:

(1) $BSFC_E$, θ_F and θ_C are sensitive to spark timing under OFC mode for all the fuel conditions (E0, E25 and E50).

(2) With a fixed spark timing, the φ_{CA50} of E50 and E25 is about 4.5 degrees and 1.9 degrees later than that of E0, respectively. θ_F and θ_C can be extended with the increase of ethanol fraction in the blended fuel.

(3) With MBT timing under each OMF condition, by increasing OMF from 23.3% to 29%, the saving rate of $BSFC_E$ is 2.12%, 1.65% and 1.51% for E0, E25 and E50, respectively. The corresponding increase in BSOC is each 21.83%, 22.42% and 22.58%, which should also

increase the attention in the practical applications.

(4) θ_F, θ_C and HRR are not sensitive to OMF. With the increase of OMF, the increment of θ_F is each 0.7 degrees, 1.8 degrees and 2.2 degrees for E0, E25 and E50. θ_C is only extended by 1 degree, 1.1 degrees and 1.4 degrees, respectively.

(5) By increasing T_I from 298 K to 358 K, $BSFC_E$ and BSOC present steady but slight growth trends under all the fuel conditions. θ_F and θ_C could be slightly reduced, meantime φ_{CA50}, φ_{Pmax} and the position of HRR peak could be advanced by nearly 1 degree.

In the future, more research about OFC in GDI engines fuelled with gasoline-ethanol blends would be beneficial. For example, further studies could include other new parameters, such as the effects of variable valve actuation strategies, Exhaust Gas Recirculation (EGR), intake pressure and temperatures, fuel injection rate and pressure, etc. Besides, the studies about combustion performance under some other representative load points can also be considered. Thus, future works can further benefit the implementation of OFC in GDI engines fuelled with gasohol, providing a practical and meaningful way to help achieve zero carbon emissions from ICE.

AUTHOR INFORMATION

Corresponding Author:

Xiang Li, School of Computer Science and Technology, University of Bedfordshire, Luton, LU1 3JU, UK; orcid.org/0000-0002-4442-9330; Email: xiang.li@beds.ac.uk

Zhijun Peng, School of Engineering, University of Lincoln, Lincoln, LN6 7TS, UK. Email: jpeng@lincoln.ac.uk

Authors:

Yiqiang Pei, State Key Laboratory of Engines, Tianjin University, Tianjin 300072, China

Dayou Li, School of Computer Science and Technology, University of Bedfordshire, Luton, LU1 3JU, UK

Tahmina Ajmal, School of Computer Science and Technology, University of Bedfordshire, Luton, LU1 3JU, UK

Abdel Aitouche, [1] Univ. Lille, CNRS, Centrale Lille, UMR 9189 - CRIStAL - Centre de Recherche en Informatique Signal et Automatique de Lille, F-59000 Lille, France. [2] Junia, Smart Systems and Energies, F-59000 Lille, France.

Raouf Mobasheri, [1] Univ. Lille, CNRS, Centrale Lille, UMR 9189 - CRIStAL - Centre de Recherche en Informatique Signal et Automatique de Lille, F-59000 Lille, France. [2] Junia, Smart Systems and Energies, F-59000 Lille, France.

ACKNOWLEDGEMENTS

This work is financially supported by European Regional Development Fund (ERDF) via Interreg North-West Europe (Project No. NWE553).

REFERENCES

[1] Salvia, M.; Reckien, D.; Pietrapertosa, F.; Eckersley, P.; Spyridaki, N.A.; Krook-Riekkola, A.; Olazabal, M.; Hurtado, S.D.G.; Simoes, S.G.; Geneletti, D.; et al. Will climate mitigation ambitions lead to carbon neutrality? An analysis of the local-level plans of 327 cities in the EU. *Renewable Sustainable Energy Rev.* 2021, 135: 110253.

[2] Koytsoumpa, E.I.; Bergins, C.; Kakaras, E. The CO_2 economy: Review of CO_2 capture and reuse technologies. *J. Supercrit. Fluids* 2018, 132: 3-16.

[3] Anwar, M.N.; Fayyaz, A.; Sohail, N.F.; Khokhar, M.F.; Baqar, M.; Khan, W.D.; Rasool, K.; Rehan, M.; Nizami, A.S. CO2 capture and storage: a way forward for sustainable environment. *J. Environ. Manage.* 2018, 226: 131-144.

[4] Zheng, G.; Peng, Z. Life Cycle Assessment (LCA) of BEV's environmental benefits for meeting the challenge of ICExit (Internal Combustion Engine Exit). *Energy Reports* 2021, 7: 1203-1216.

[5] Yaverbaum, L. Fluidized bed combustion of coal and waste materials. *NASA STI/Recon Technical Report A* 1977, 78: 33803.

[6] Bilger, R.W. Zero release combustion technologies and the oxygen economy. *Fifth International Conference on Technologies and Combustion for a Clean Environment, Lisbon, Portugal, Jul* 1999: 12-15.

[7] Wu, H.W.; Wang, R.H.; Chen, Y.C.; Ou, D.J.; Chen, T.Y. Influence of port-inducted ethanol or gasoline on combustion and emission of a closed cycle diesel engine. *Energy* 2014, 64: 259-267.

[8] Li, X.; Peng, Z.; Ajmal, T.; Aitouche, A.; Mobasheri, R.; Pei, Y.; Gao, B.; Wellers, M. A feasibility study of implementation of oxy-fuel combustion on a practical diesel engine at the economical oxygen-fuel ratios by computer simulation. *Adv. Mech. Eng.* 2020, 12(12): 1687814020980182.

[9] Wall, T.; Liu, Y.; Spero, C.; Elliott, L.; Khare, S.; Rathnam, R.; Zeenathal, F.; Moghtaderi, B.; Buhre, B.; Sheng, C.; et al. An overview on oxyfuel coal combustion—State of the art research and technology development. Chem. *Eng. Res. Des.* 2009, 87(8): 1003-1016.

[10] Chen, L.; Yong, S.Z.; Ghoniem, A.F. Oxy-fuel combustion of pulverized coal: Characterization, fundamentals, stabilization and CFD modeling. *Prog. Energy Combust. Sci.* 2012, 38(2): 156-214.

[11] Yu, X.; Wu, Z.; Wang, C.; Deng, J.; Hu, Z.; Li, L. *Study of the combustion and emission characteristics of a quasi ICRC engine under different engine loads*. SAE Technical Paper 2014-01-1202, SAE, 2014.

[12] Fu, L.Z.; Wu, Z.; Li, L.; Yu, X. *Effect of Water Injection Temperature on Characteristics of Combustion and Emissions for Internal Combustion Rankine Cycle Engine*. SAE Technical Paper 2014-01-2600, SAE, 2014.

[13] Wu, Z.J.; Yu, X.; Fu, L.Z.; Deng, J.; Hu, Z.J.; Li, L.G. A high efficiency oxyfuel internal combustion engine cycle with water direct injection for waste heat recovery. *Energy* 2014, 70: 110-120.

[14] Wu, Z.J.; Yu, X.; Fu, L.Z.; Deng, J.; Li, L.G. Experimental study of the effect of water injection on the cycle performance of an internal-combustion Rankine cycle engine. *Proc. Inst. Mech. Eng., Part D* 2014, 228(5): 580-588.

[15] Li, X.; Peng, Z.; Ajmal, T.; Rana, K.J.; Aitouche, A.; Mobasheri, R.; Pei, Y. *Simulation Study on Implementation of Oxy-Fuel Combustion for a Practical GDI Engine*. SAE Technical Paper 2021-01-0380, SAE, 2021.

[16] Li, X.; Pei, Y.; Peng, Z.; Ajmal, T.; Rana, K.J.; Aitouche, A.; Mobasheri, R. Numerical study on the effects of intake charge on oxy-fuel combustion in a dual-injection spark ignition engine at economical oxygen-fuel ratios. *Int. J. Engine Res.* 2021: 14680874211022292.

[17] An, Y.; Teng, S.; Li, X.; Qin, J.; Zhao, H.; Zhan, Z.S.; Hu, T.G.; Liu, B.; Zhong, J. *Study of polycyclic aromatic hydrocarbons evolution processing in GDI engines using TRF-PAH chemical kinetic mechanism*. SAE Technical Paper 2016-01-0690, SAE, 2016.

[18] Wu, M.; Pei, Y.; Qin, J.; Li, X.; Zhou, J.; Zhan, Z.S.; Guo, Q.Y.; Liu, B.; Hu, T.G. *Study on methods of coupling numerical simulation of conjugate heat transfer and in-cylinder combustion process in GDI engine*. SAE Technical Paper 2017-01-0576, SAE, 2017.

[19] Kim, T.; Song, J.; Park, J.; Park, S. Numerical and experimental study on effects of fuel injection timings on combustion and emission characteristics of a direct-injection spark-ignition gasoline engine with a 50 MPa fuel injection system. *Appl. Therm. Eng.* 2018, 144: 890-900.

[20] Duronio, F.; De Vita, A.; Allocca, L.; Anatone, M. Gasoline direct injection engines–A review of latest technologies and trends. Part 1: Spray breakup process. *Fuel* 2020, 265: 116948.

[21] Wang, C.; Pei, Y.; Qin, J.; Peng, Z.; Liu, Y.; Xu, K.; Ye, Z. Laser induced fluorescence investigation on deposited fuel film from spray impingement on viscous film over a solid wall. *Energy* 2021, 231: 120893.

[22] Choi, Y.; Yi, H.; Oh, Y.; Park, S. Effects of engine restart strategy on particle number emissions from a hybrid electric vehicle equipped with a gasoline direct injection engine. *Atmos. Environ.* 2021, 253: 118359.

[23] Wang, Z.; Liu, H.; Long, Y.; Wang, J.; He, X. Comparative study on alcohols–gasoline and gasoline–alcohols dual-fuel spark ignition (DFSI) combustion for high load extension and high fuel efficiency. *Energy* 2015, 82: 395-405.

[24] Huang, H.; Wang, Q.; Shi, C.; Liu, Q.; Zhou, C. Comparative study of effects of pilot injection and fuel properties on low temperature combustion in diesel engine under a medium EGR rate. *Appl. Energy* 2016, 179: 1194-1208.

[25] Huang, H.; Teng, W.; Li, Z.; Liu, Q.; Wang, Q.; Pan, M. Improvement of emission characteristics and maximum pressure rise rate of diesel engines fueled with n-butanol/PODE3-4/diesel blends at high injection pressure. *Energy Convers. Manage.* 2017, 152: 45-56.

[26] Li, X.; Pei, Y.Q.; Qin, J.; Zhang, D.; Wang, K.; Xu, B. Effect of ultra-high injection pressure up to 50 MPa on macroscopic spray characteristics of a multi-hole gasoline direct injection injector fueled with ethanol. *Proc. Inst. Mech. Eng., Part D* 2018, 232(8): 1092-1104.

[27] Huang, H.; Liu, Q.; Teng, W.; Pan, M.; Liu, C.; Wang, Q. Improvement of combustion performance and emissions in diesel engines by fueling n-butanol/diesel/PODE3–4 mixtures. *Appl. Energy* 2018, 227: 38-48.

[28] Venu, H.; Raju, V.D.; Subramani, L. Combined effect of influence of nano additives, combustion chamber geometry and injection timing in a DI diesel engine fuelled with ternary (diesel-biodiesel-ethanol) blends. *Energy* 2019, 174: 386-406.

[29] Huang, H.; Zhu, Z.; Chen, Y.; Chen, Y.; Lv, D.; Zhu, J.; Ouyang, T. Experimental and numerical study of multiple injection effects on combustion and emission characteristics of natural gas–diesel dual-fuel engine. *Energy Convers. Manage.* 2019, 183: 84-96.

[30] Holman, J.P. Experimental methods for engineers. *Mc Grawhill* 1966.

[31] Liu, K.; Li, Y.; Yang, J.; Deng, B.; Feng, R.; Huang, Y. Comprehensive study of key operating parameters on combustion characteristics of butanol-gasoline blends in a high speed SI engine. *Appl. Energy* 2018, 212: 13-32.

[32] Tornatore, C.; Bozza, F.; De Bellis, V.; Teodosio, L.; Valentino, G.; Marchitto, L. Experimental and numerical study on the influence of cooled EGR on knock tendency, performance and emissions of a downsized spark-ignition engine. *Energy* 2019, 172: 968-976.

[33] Tian, Z.; Zhen, X.; Wang, Y.; Liu, D.; Li, X. Combustion and emission characteristics of n-butanol-gasoline blends in SI direct injection gasoline engine. *Renewable Energy* 2020, 146: 267-279.

[34] Woschni, G. *A universally applicable equation for the instantaneous heat transfer coefficient in the internal combustion engine*. SAE Technical paper 670931, SAE,1967.

[35] Heywood, J.B. Internal Combustion Engine Fundamentals (2nd edit). *McGraw-Hill* 2018.

[36] Metghalchi, M.; Keck, J.C. Burning velocities of mixtures of air with methanol, isooctane, and indolene at high pressure and temperature. *Combust. Flame* 1982, 48: 191-210.

Appendix

Abbreviations

BMEP	Brake Mean Effective Pressure
BSFC	Brake Specific Fuel Consumption
CA	Crank Angle
CAC	Conventional Air Combustion
CCS	Carbon Capture and Storage
CO_2	Carbon Dioxide
E0	gasoline
E25	25% ethanol, 75% is gasoline in mass fraction
E50	50% ethanol, 50% is gasoline in mass fraction
ECU	Electronic Control Unit
EGR	Exhaust Gas Recirculation
ERDF	European Regional Development Fund
GDI	Gasoline Direct Injection
GHG	Greenhouse Gas
HRR	Heat Release Rate
ICE	Internal Combustion Engine
ICRC	Internal Combustion Rankine Cycle
KLSA	Knock Limited Spark Advance
MBT	Maximum Brake Torque
OFC	Oxy-Fuel Combustion
OMF	Oxygen Mass Fraction
PFI	Port Fuel Injection
rpm	revolutions per minute
SI	Spark Ignition

For Table of Contents Only